

## Morphology control of NiCo<sub>2</sub>O<sub>4</sub>/NF materials by surfactant addition and its electrochemical properties

Lifei Zhi<sup>1,\*</sup>, Shushan Yao<sup>2</sup>, Eezhuang Zhang<sup>1</sup>, Mingang Zhang<sup>2</sup>

<sup>1</sup> College of Chemistry and Biological Engineering, Taiyuan University of Science and Technology, Taiyuan 030024, China;

<sup>2</sup> School of Materials Science and Engineering, Taiyuan University of Science and Technology, Taiyuan 030024, China

\*E-mail: [lifeizhi@yeah.net](mailto:lifeizhi@yeah.net)

Received: 22 April 2022 / Accepted: 27 May 2022 / Published: 4 July 2022

---

Micro–nanostructured NiCo<sub>2</sub>O<sub>4</sub> with controllable *in situ* growth on foam nickel has been successfully realized by introducing different surfactants as soft templates. Herein, several self-supporting NiCo<sub>2</sub>O<sub>4</sub>/NF electrode materials with different dimensions, different morphologies, and excellent electrochemical properties were prepared. The effects of the surfactant type, structure, and reaction conditions on the morphologies, structures, and electrochemical properties of the materials were studied in detail. The results show that NiCo<sub>2</sub>O<sub>4</sub> materials can regulate the formation of flake and fibrous structures of different sizes using a linear anionic surfactant. With the increase in temperature, the cationic surfactant (DMHAC10) can regulate the formation of flake → cactus → fibrous structure. Also, the Gemini cationic surfactant (GC-A) can regulate the formation of flake → cactus ball → urchin-like → fibrous structure. The growth of NiCo<sub>2</sub>O<sub>4</sub> on NF was prevented due to nonionic surfactants. Counter ions only affect the size of the material structure, but the material morphology is unaffected, and the surfactant concentration slightly affects the material morphology. The results of the electrochemical properties showed that the cactus ball NiCo<sub>2</sub>O<sub>4</sub>/NF material of a three-dimensional multistage structure was prepared by adding GC-A at 120°C for 6 h. The prepared material has excellent electrochemical properties such as higher specific capacity (4.74 F/cm<sup>2</sup>), better charge–discharge ratio, and better cycle stability.

---

**Keywords:** Surfactant; Nickel cobaltite; Morphology control; Electrochemical properties; Soft templates

### 1. INTRODUCTION

NiCo<sub>2</sub>O<sub>4</sub> has attracted significant interest because of its unique magnetic, electrical, optical, and catalytic properties, environmental friendliness, and cost-effectiveness. It has tremendous

application prospects in catalysts, supercapacitors, sensors, and lithium-ion batteries [1-3]. However, nanoNiCo<sub>2</sub>O<sub>4</sub> materials with different morphologies and sizes have different magnetic, electrical, and optical properties, and can be applied to various fields. NiCo<sub>2</sub>O<sub>4</sub> materials with porous network structures and large specific surface areas are advantageous in improving electrolyte permeability and ion transfer. Therefore, it has excellent application prospects in supercapacitors and lithium-ion batteries [4]. Nanofibrous-structured NiCo<sub>2</sub>O<sub>4</sub> exhibits high catalytic activity in oxygen production from electrolytic water. However, by only realizing the controllable morphological growth, size, growth direction, and growth position, NiCo<sub>2</sub>O<sub>4</sub> materials can obtain the structure and properties for targeted applications [5, 6]. Therefore, the preparation technology from “random growth” to “controllable growth” is essential.

In soft template systems, the space confinement ability and intermolecular forces guide and regulate the regular self-assembly of free precursors to control the structure, size, orientation, composition, arrangement, and morphology of materials [7-9]. In the soft template method, it is easy to remove the later template, and the template fragments can be recycled [10]. Surfactants can accumulate in solution to form ordered aggregates, such as micelles, vesicles, and microemulsions [11]; thus, playing a “microreactor” soft template role in the preparation of nanomaterials [12]. Surfactants can also be used as stabilizers to prevent rapid adsorption and agglomeration at the initial stage of nanocrystalline seed formation. Additionally, surfactants can be selectively adsorbed to a surface of the crystal nucleus, limiting the accumulation of reducing particles on that surface, promoting the growth of atoms on the other surface, and guiding the direction of particle accumulation [13]. Therefore, surfactants play a crucial role in the morphology control and size design of functional nanomaterials [14, 15].

Surfactant molecules have hydrophilic and hydrophobic groups, so they have good solubility in aqueous solutions and organic solvents, which is very easy for later removal [16]. As a soft template, the amount of surfactant added to the system is minimal and slightly affects the production cost. Therefore, this method has broad application prospects for the industrialized production of controllable shape materials.

Therefore, surfactants are used as special microreactors for soft templates to enable NiCo<sub>2</sub>O<sub>4</sub> materials to achieve “controllable *in situ* growth” on foamed nickel. Three types of surfactants, including cationic, anionic, and nonionic surfactants, were used as soft templates to systematically study the morphology control of *in situ* grown self-supporting NiCo<sub>2</sub>O<sub>4</sub>/NF composite electrode materials on foam nickel substrates, and explore the controllable growth mechanism. The electrochemical properties of NiCo<sub>2</sub>O<sub>4</sub>/NF composites with different morphologies were studied using cyclic voltammetry (CV), impedance tests, and constant current charge–discharge.

## 2. EXPERIMENTAL

### 2.1 Materials

Ni(NO<sub>3</sub>)<sub>2</sub>·6H<sub>2</sub>O, AR, Shanghai MACKLIN Biochemical Technology Co., Ltd.. Co(NO<sub>3</sub>)<sub>2</sub>·6H<sub>2</sub>O, AR, Aladdin Reagent Co., Ltd.. Urea and ammonium fluoride, AR, Shanghai Er Bi Chemical Reagent Co., Ltd.. HCl, AR, China Pharmaceutical Group Chemical Reagent Co., Ltd..

NaOH and absolute alcohol, AR, Tianjin Chemical Reagent Co., Ltd., Tianjin. Ni foam (1 cm × 2.0 cm), Shenzhen Feixin Filter Equipment Co. Ltd.. Modified oil ethoxylate sodium sulfonate (SNS-80, 100%), Fatty alcohol polyoxyethylene ether (AEO<sub>9</sub>, 100%), and alkyl glycoside 12-14 (APG12-14, 50%) were purchased from China Light Daily Chemical Technology Co., Ltd. Sodium dodecyl sulfate (K12, AR), Fatty alcohol polyoxyethylene ether sulfate (AES, AR), N-Decyl-N-(2-hydroxyethyl)-N-methyldecan-1-aminium chloride (DMHAC10, AR), N, N-dimethyl dodecyl/tetradecyl tertiary amine Gemini (GC-A, 40%), N-Decyl-N,N-dimethyldecan-1-aminium formate (DDAF, 81%), N-Decyl-N,N-dimethyldecan-1-aminium valerate (DDAV, 82%), N-Decyl-N,N-dimethyldecan-1-aminium propionate (DDAP, 77.5%), N-Decyl-N,N-dimethyldecan-1-aminium butyrate (DDAB, 75%), N-Decyl-N,N-dimethyldecan-1-aminium chloride (DDAC, 87%) is provided by China research institute of daily chemical industry.

## 2.2 Equipment

Powder X-ray diffraction (XRD), Germany Bruker Co., Ltd. Field emission scanning electron microscope (SEM s-4800), Japan Hitachi Co., Ltd. Automatic specific surface area tester (ASAP 2010), USA micromeritics Co., Ltd. Full automatic surface tension meter (JK99C), Shanghai Zhongchen digital technology equipment Co., Ltd. Electrochemical workstation (CHI660E), Shanghai Chenhua Co., Ltd.

## 2.3 Preparation of NiCo<sub>2</sub>O<sub>4</sub>/NF composites

NiCo<sub>2</sub>O<sub>4</sub>/NF material was prepared by hydrothermal method. First, The Ni foam (1 cm × 2.0 cm) were cleaned by ultrasonication in 3 M HCl aqueous solution to remove the NiO layer, then washed carefully with absolute ethanol and deionized water for 30 min. Secondly, CO(NO<sub>3</sub>)<sub>2</sub>·6H<sub>2</sub>O (1.32 mmol), Ni (NO<sub>3</sub>)<sub>2</sub>·6 H<sub>2</sub>O (0.366 mmol), urea (20.0 mmol), NH<sub>4</sub>F (8.0 mmol) and surfactant (0.05 g) were dissolved and dispersed in deionized water (40 ml). Finally, the Ni foam and the above mixed solution were transferred into 50 ml Teflon-lined stainless steel autoclave. The reaction was carried out at a certain temperature for 6 h, it was dried at 60 °C for 12 h, and then calcined at 300 °C in air for 2 h.

## 2.4 Material characterization

The crystalline structure of the product was examined by XRD with graphite monochromator and Cu Ka X-ray, working voltage 40 kV, acceleration current 100 mA, 2θ=10° to 80°, and the scanning speed is 4 °/min. The specific surface area and pore volume and pore size distribution were measured by N<sub>2</sub> adsorption desorption isotherm, degassed at 120 °C for 8 h under vacuum, and the sample cell temperature was 77 K.

### 2.5 Surface tension measurement

The surface tension was measured by ring method. It needs to be calibrated with ultrapure water before each measurement of surface tension. The temperature was  $25.0 \pm 0.1$  °C, and the surface tension measurements were conducted five times, with a 2min interval between each reading.

### 2.6 Electrochemical measurements

The scanning range of the CV measurements was 10.0–50.0 mV/s, and the frequency range of the impedance test was 0.01–10 kHz. A three-electrode system was used for all tests in 6.0 M KOH aqueous solution. The working, reference, and symmetrical electrodes were NiCo<sub>2</sub>O<sub>4</sub>/NF composite, calomel electrode, and platinum sheet, respectively. The specific capacitance (C, F/cm<sup>2</sup>) was calculated from the CV Curve and Equation (1) [17, 18].

$$C = \frac{1}{sv(V_c - V_a)} \int_{V_a}^{V_c} I(V) dV \quad (1)$$

Here,  $s$  represents the area of the electrode material (cm<sup>2</sup>),  $v$  represents the scanning rate (mV/s),  $V_a$  and  $V_c$  represent the anode and cathode potentials (V), respectively,  $I$  represents the current (A), and  $V$  represents the potential (V). The constant current charge–discharge test was conducted on the Wuhan blue electric test system (LAND-CT2001A). The specific capacitance (C, F/cm<sup>2</sup>) was calculated using Equation (2) [19] as follows:

$$Cs = (I \times t) / s \Delta V \quad (2)$$

Here,  $I$  represents the constant current discharge current (A),  $s$  represents the area of the electrode material (cm<sup>2</sup>),  $\Delta V$  represents the voltage drop during discharge (V), and  $t$  represents the discharge time (s).

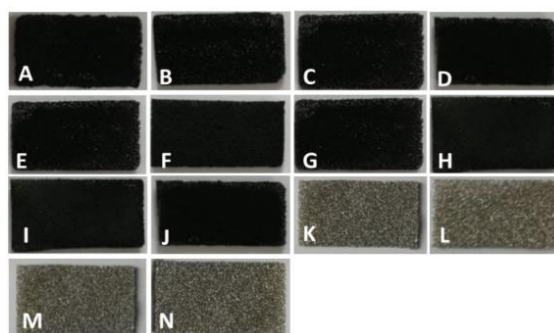
## 3. RESULTS AND DISCUSSION

### 3.1 XRD characterization

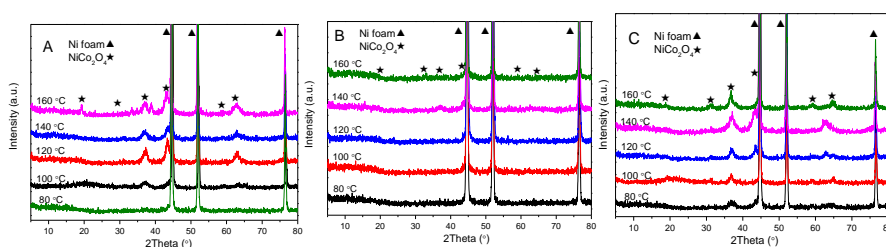
Cationic, anionic, and nonionic surfactants were added as soft templates during the preparation of the NiCo<sub>2</sub>O<sub>4</sub>/NF materials, and were investigated at different reaction temperatures (80°C, 100°C, 120°C, 140°C, and 160°C). The NiCo<sub>2</sub>O<sub>4</sub>/NF sheet prepared at 180°C was corroded into fragments, so the maximum temperature of the reaction was 160°C. The names and molecular and structural formulas of the surfactants are presented in the Supporting Materials. Surfactants DDAF, DDAP, DDAB, DDAV, DDAC, DMHAC10, and GC-A are cationic surfactants. Sodium dodecyl sulfate (K12, CH<sub>3</sub>(CH<sub>2</sub>)<sub>11</sub>OSO<sub>3</sub>Na), fatty alcohol polyoxyethylene ether sodium sulfate (AES, CH<sub>3</sub>(CH<sub>2</sub>)<sub>11</sub>O(CH<sub>2</sub>CH<sub>2</sub>O) <sub>$n$</sub> -SO<sub>3</sub>Na ( $n = 2$  or  $3$ )), and SNS-80 are anionic surfactants [20]. APG and AEO<sub>9</sub> are nonionic surfactants [21]. The optical images of NiCo<sub>2</sub>O<sub>4</sub>/NF in Fig. 1 show that the colors of the Ni foam materials with no surfactants, cationic surfactants, and anionic surfactants (K12 and AES) changed from silver to black, and the color distribution was more uniform. These results indicate that new materials were grown on the surface of the Ni foam, and the growth distribution

was more uniform (Fig. 1(A)–(J)). The appearance of the samples prepared by adding nonionic surfactants (APG and AEO9) and anionic surfactant SNS-80 was silver (in the temperature range investigated). The results indicate that the addition of the three surfactants inhibited the formation of NiCo<sub>2</sub>O<sub>4</sub> on the surface of the Ni foam.

The XRD spectra of the NiCo<sub>2</sub>O<sub>4</sub>/NF samples obtained by adding different soft templates (K12, AES, DMHAC10, and GC-A) at different reaction temperatures are shown in Fig. 2. Fig. 2(E) shows the XRD spectra of the products obtained using several cationic surfactants (DDAF, DDAC, DDAP, DDAB, DDAV) soft templates at 100°C for 6 h. The three-strong diffraction peaks (44.7°, 52.1°, and 76.6°) are shown, which are assigned to the (111), (200), and (220) planes of Ni (JCPDS card No. 04-0850) [22], respectively. Additionally, there are other diffraction peaks at 18.9°, 30.8°, 36.8°, 43.8°, 59°, and 64.8°, which are assigned to the (111), (220), (311), (400), (511), and (440) planes of NiCo<sub>2</sub>O<sub>4</sub> (Fig. 2(A) and (C)–(F)) (JCPDS Card No. 73-1702), respectively [23]. In Fig. 2(B), these characteristic peaks are not obvious because the Ni peak is particularly strong, covering up the diffraction peak of NiCo<sub>2</sub>O<sub>4</sub> [24]. Also, Fig. 2(C) shows that the peak shape is sharp in the presence of DMHAC10, indicating that NiCo<sub>2</sub>O<sub>4</sub> crystal is highly crystalline. Moreover, it can be observed from Fig. 2 that the XRD diffraction peak intensity of NiCo<sub>2</sub>O<sub>4</sub> increases as the reaction temperature increases. This phenomenon shows that the crystallization degree of NiCo<sub>2</sub>O<sub>4</sub> increases as the reaction temperature increases. According to the Scherrer equation, when K12 is added in Fig. 2(A), the average particle sizes of the NiCo<sub>2</sub>O<sub>4</sub> particles are 26.2, 29.3, 28.5, 32.1, and 34.5 nm at 80°C, 100°C, 120°C, 140°C, and 160°C respectively. These results show that NiCo<sub>2</sub>O<sub>4</sub>/NF composite electrode materials were successfully prepared by adding these anionic and cationic soft templates.



**Figure 1.** The appearance of NiCo<sub>2</sub>O<sub>4</sub> material in situ grown on Ni foam. A: no surfactant; B: K12; C: AES; D: DMHAC10; E: GC-A; F: DDAF; G: DDAC; H: DDAP; I: DDAB; J: DDAV; K: SNS-80; L: APG; M: AEO<sub>9</sub>; N: Nickel foam.



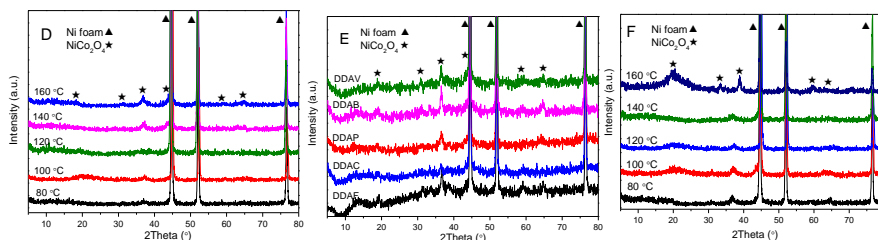


**Figure 2.** XRD spectrum of NiCo<sub>2</sub>O<sub>4</sub>/NF. A: K12, B: AES, C: DMHAC10, D: GC-A, E:100 °C, 6 h, F: no surfactant

### 3.2 Morphology of NiCo<sub>2</sub>O<sub>4</sub>/NF

The morphologies of the NiCo<sub>2</sub>O<sub>4</sub>/NF composite electrode materials prepared without surfactants are shown in Fig. 3(A)–(E). All NiCo<sub>2</sub>O<sub>4</sub> samples show nanosheet structures at different reaction temperatures. As the temperature increases, the thicknesses of the nanosheets decrease, the diameters decrease, the densities of the nanoarray structures increase, and the hole sizes decrease. The results show that adjusting the reaction temperature slightly affects the morphology of NiCo<sub>2</sub>O<sub>4</sub>, and the material prepared using this method has a single structure.

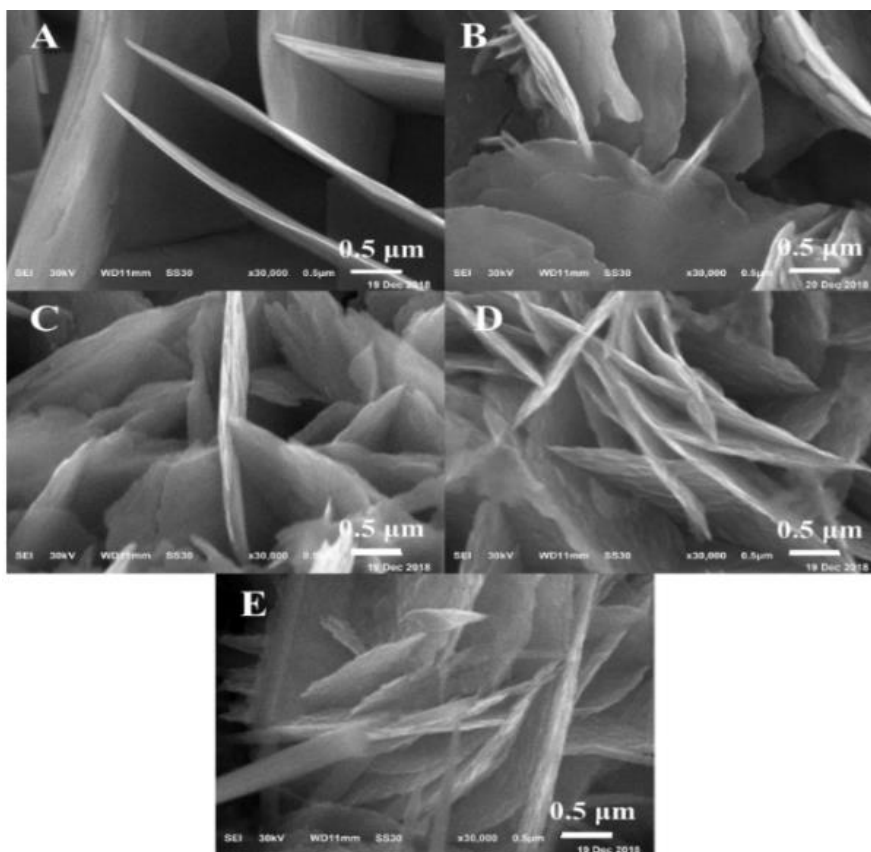


**Figure 3.** The SEM images of the NiCo<sub>2</sub>O<sub>4</sub>/NF (A) 80 °C, (B) 100 °C, (C) 120 °C, (D) 140 °C, (E) 160 °C

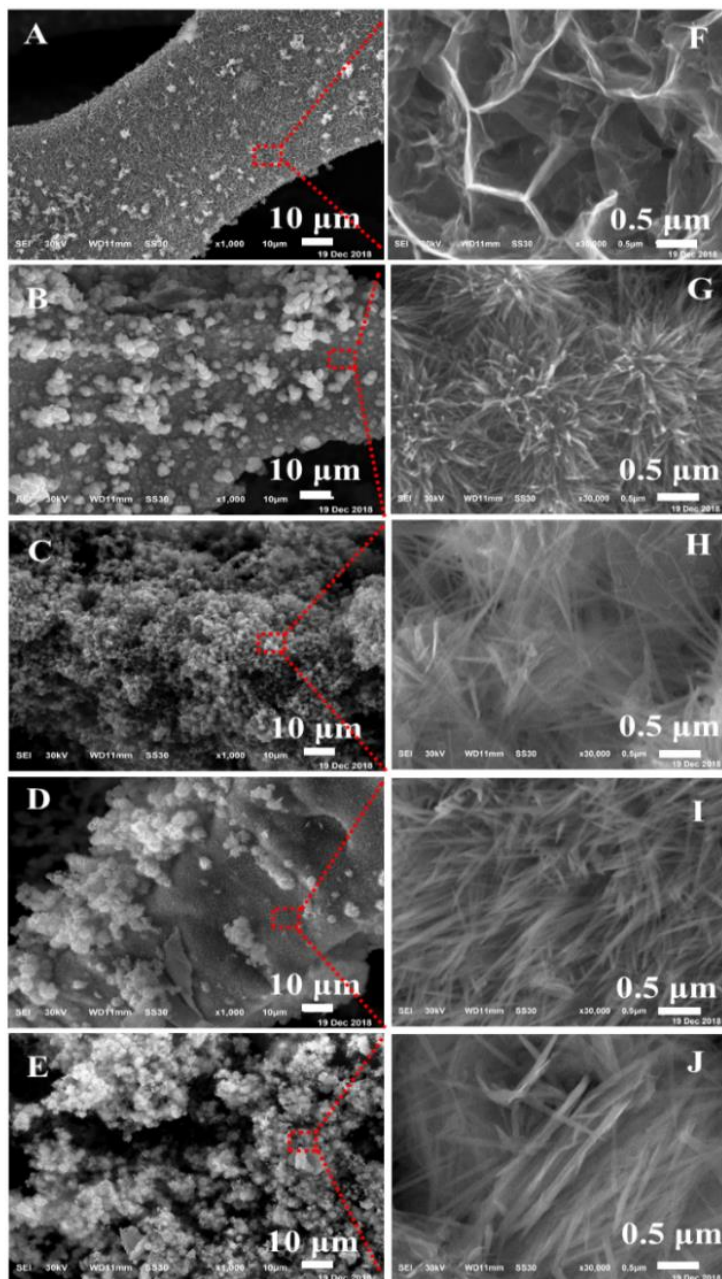


**Figure 4.** The SEM images of NiCo<sub>2</sub>O<sub>4</sub>/NF adding K12. (A, F) 80 °C, (B, G) 100 °C, (C, H) 120 °C, (D, I) 140 °C, (E, J) 160 °C

Fig. 4 shows the scanning electron microscopy (SEM) images of the NiCo<sub>2</sub>O<sub>4</sub>/NF materials prepared by adding K12 at different temperatures. As shown in Fig. 4(A)–(E), the formation of new materials with different morphologies on the Ni foam skeletons of all samples indicates that the prepared NiCo<sub>2</sub>O<sub>4</sub> was directly grown on the skeletons of the Ni foam materials. The morphology of the grown NiCo<sub>2</sub>O<sub>4</sub> is amplified (Fig. 4(F)–(J)). Also, the morphology of NiCo<sub>2</sub>O<sub>4</sub> changes on the Ni foam skeleton with varying reaction temperatures. Evidently, at a low reaction temperature (Fig. 4(F)), the NiCo<sub>2</sub>O<sub>4</sub>/NF material is of the flocculent structure. As the reaction temperature increases, nanofibrous structures are observed. Furthermore, longer and larger fibrous structures are observed

at elevated reaction temperatures. The nanofibrous  $\text{NiCo}_2\text{O}_4$  material has high catalytic activity in oxygen production from electrolytic water [25, 26]. Therefore, the fibrous  $\text{NiCo}_2\text{O}_4/\text{NF}$  materials prepared with the K12 soft template have broad potential application prospects in oxygen production from electrolytic water.

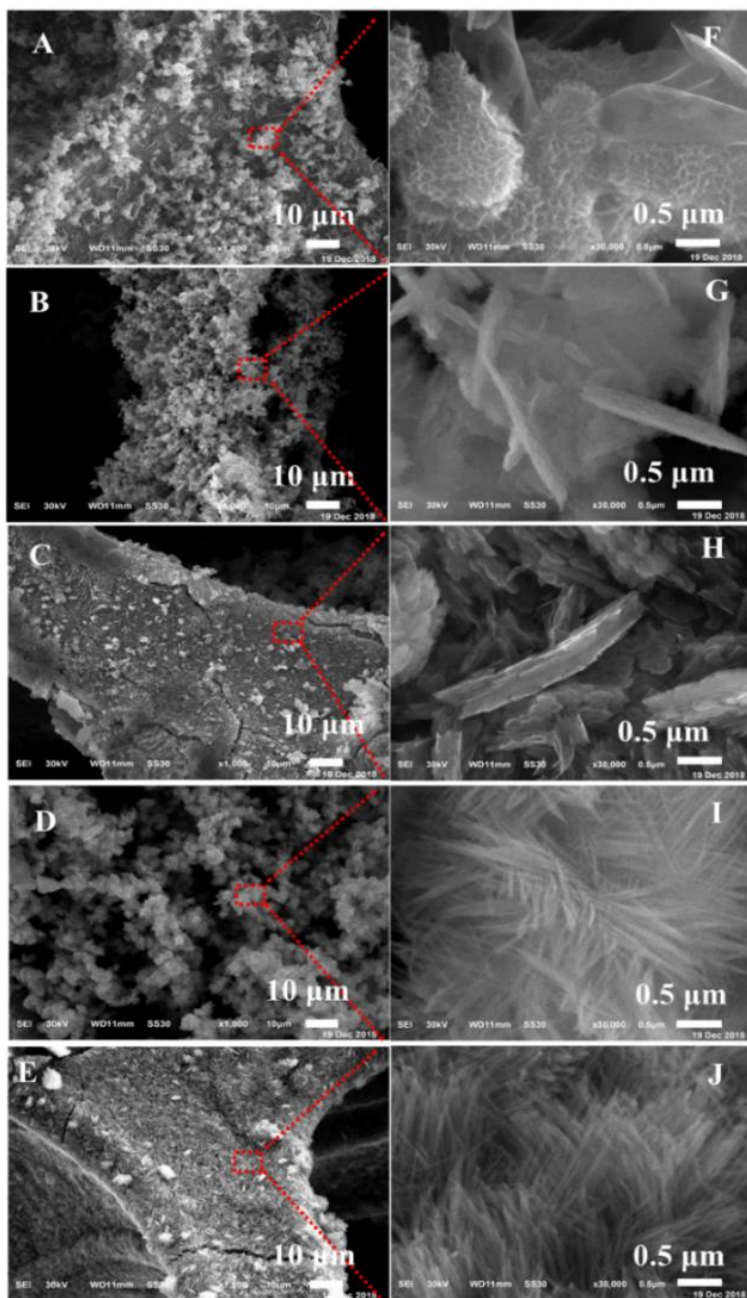


**Figure 5.** The SEM images of  $\text{NiCo}_2\text{O}_4/\text{NF}$  adding AES (A, F) 80 °C, (B, G) 100 °C, (C, H) 120 °C, (D, I) 140 °C, (E, J) 160 °C

The SEM images of the  $\text{NiCo}_2\text{O}_4/\text{NF}$  materials prepared by adding AES as the soft template are shown in Fig. 5. Fig. 5(A)–(E) show that all samples have new substances of different morphologies on the Ni foam skeleton. The morphology of the  $\text{NiCo}_2\text{O}_4/\text{NF}$  material is both flake and spherical, and the

structural order is low under a reaction condition of 80°C for 6 h (Fig. 5(F)). At 100°C, the morphology changes to a sheet structure (Fig. 5(G)). At 120°C, the morphology is clearer (Fig. 5(H)), and the large-scale structure comprises ~0.25- $\mu\text{m}$  small scales. At 140°C and 160°C (Fig. 5(I) and (J)), fibrous structures are observed, respectively. Both AES and K12 are dodecyl linear anionic surfactants, but AES has 2–3 more ethoxy groups than K12 molecular, resulting in a different morphology of the  $\text{NiCo}_2\text{O}_4/\text{NF}$  material. Thus, Fig. 5 reveals that the composites prepared with AES as a soft template tend to form sheet and needle structures at low and high temperatures, respectively.

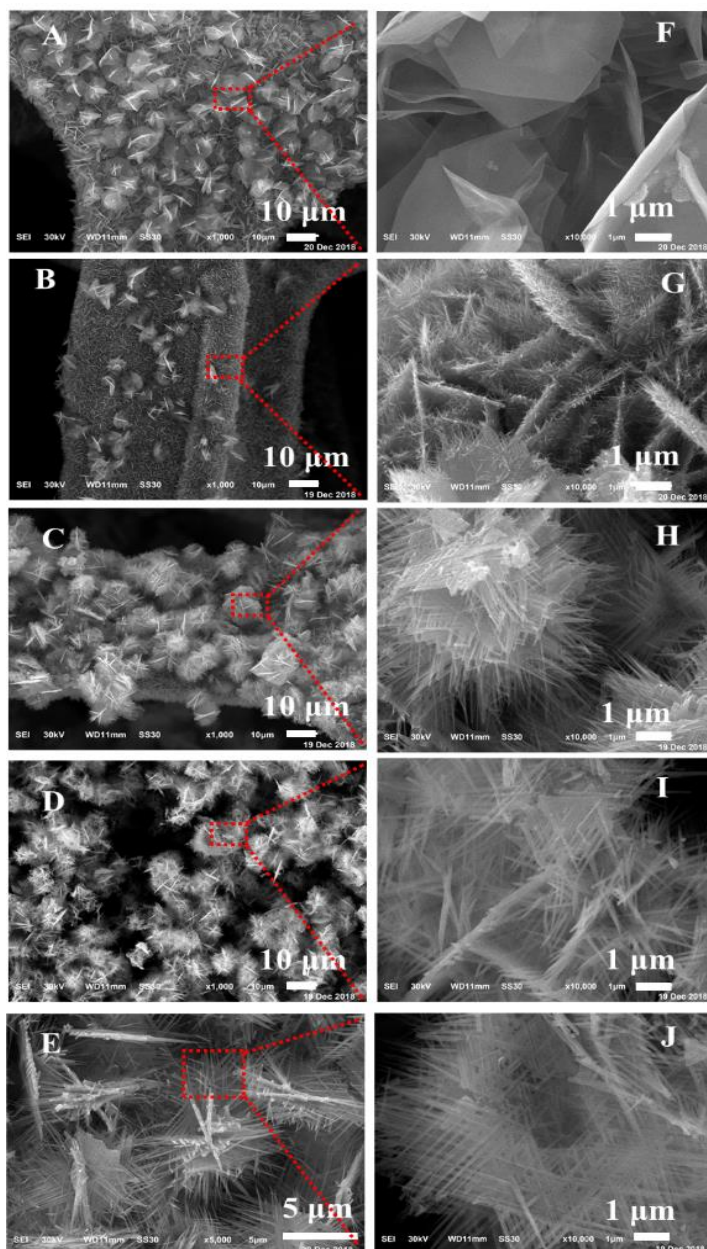


**Figure 6.** The SEM images of  $\text{NiCo}_2\text{O}_4/\text{NF}$  adding DMHAC10 (A, F) 80 °C, (B, G) 100 °C, (C, H) 120 °C, (D, I) 140 °C, (E, J) 160 °C

The SEM images of the NiCo<sub>2</sub>O<sub>4</sub>/NF composite electrode materials prepared by adding DMHAC10 as the soft template are shown in Fig. 6. Fig. 6(F) shows that the morphology of NiCo<sub>2</sub>O<sub>4</sub>/NF is of the flake structure under a reaction condition of 80°C for 6 h. As the temperature increases from 100°C to 160°C (Fig. 6(G)–(J)), mixed morphologies comprising nanofibrous and flake structures are formed. Besides, as the temperature increases, the fibrous and flake structures become clearer and less, respectively.

The SEM images of the NiCo<sub>2</sub>O<sub>4</sub>/NF materials prepared by adding GC-A as the soft template are shown in Fig. 7. The morphology of the NiCo<sub>2</sub>O<sub>4</sub>/NF material is of the sheet structure at 80°C and 100°C (Fig. 7(F) and (G)), respectively. At 120°C, it becomes a mixed morphology of cactus. Furthermore, at 140°C, the morphology comprises sea urchin microspheres, and at 160 °C, it consists of fibrous structures.

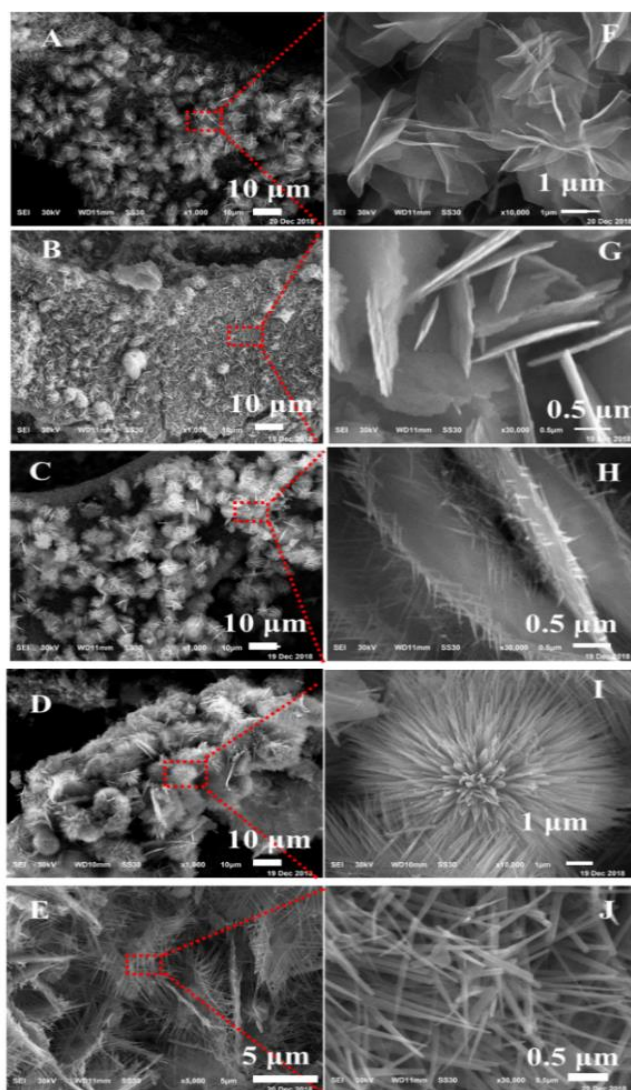


**Figure 7.** The SEM images of NiCo<sub>2</sub>O<sub>4</sub>/NF adding GC-A. (A, F) 80 °C, (B, G) 100 °C, (C, H) 120 °C, (D, I) 140 °C, (E, J) 160 °C

The SEM images of the  $\text{NiCo}_2\text{O}_4/\text{NF}$  materials prepared by adding several didecyl dimethyl cationic surfactants as the soft template at a reaction condition of  $100^\circ\text{C}$  for 6 h are shown in Fig. 8. Their counter ions range from simple  $\text{Cl}^-$  to formic acid and valerate ions. Larger flake structures are formed as the counter ions' group increases. The results show that counter ions only affect the size of the material structure, but not the morphology of the materials.

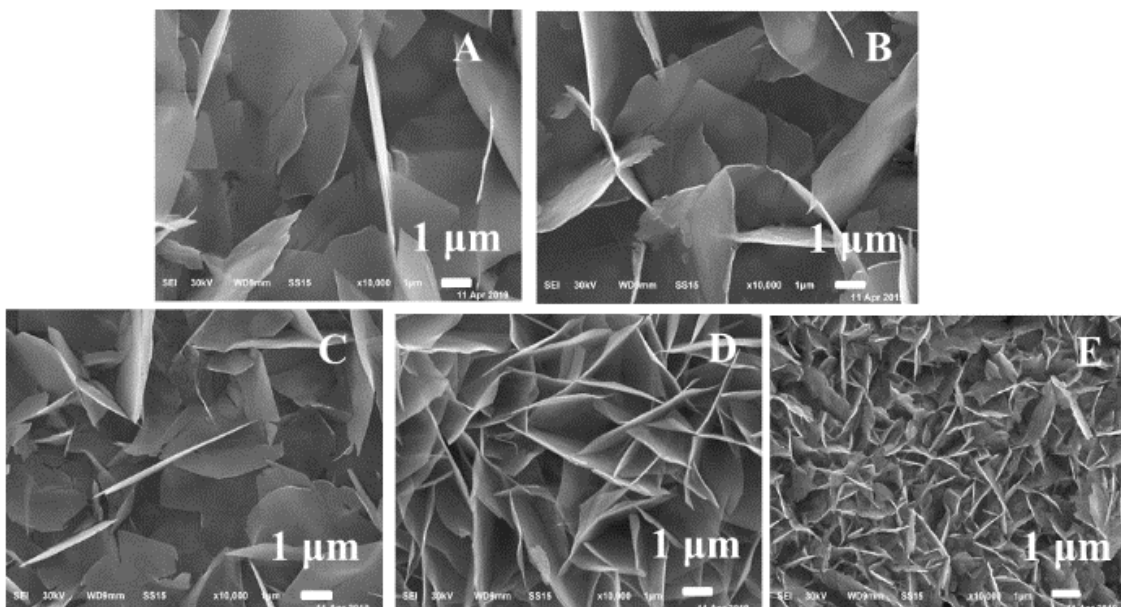


**Figure 8.** The SEM images of  $\text{NiCo}_2\text{O}_4/\text{NF}$ . A: DDAV, B: DDAB, C: DDAP, D: DDAF, E: DDAC

When the surfactant concentration exceeds the critical micelle concentration (CMC), the surfactant molecules saturate at the air–water interface. As the concentration increases, self-assembly occurs in the solution to form spherical, rod-shaped, layered, and vesicle-like aggregates and other aggregates. Thus, the function of the surfactant is demonstrated. Therefore, the concentrations of the surfactants added above exceed their respective CMC values [27, 28]. To investigate the effect of the surfactant concentration on the morphologies of the  $\text{NiCo}_2\text{O}_4/\text{NF}$  materials, the effect of the GC-A concentration on the morphologies of the  $\text{NiCo}_2\text{O}_4/\text{NF}$  materials was studied. Fig. 9 shows the relationship between the GC-A concentration and the surface tension. Evidently, the CMC value of GC-A is 0.13 mg/ml, and the surface tension is ( $\gamma$ ) 30.12 mN/m. GC-A concentrations of 0.63, 1.25, 2.5, and 3.75 mg/mL were added, respectively, which were about 5, 10, 20, and 30 times the CMC value, respectively. Fig. 10 shows the SEM images of the  $\text{NiCo}_2\text{O}_4/\text{NF}$  materials prepared by adding different concentrations of GC-A at  $100^\circ\text{C}$  for 6 h. Evidently, the morphology of the  $\text{NiCo}_2\text{O}_4/\text{NF}$  material is of the flake structure. The morphology and size of the material prepared under the concentrations of 5, 10, and 20 times the CMC value (Fig. 10(A)–(C)) are similar, and there is almost no change. When the concentration increases to 30 times the CMC value (Fig. 10(D)), the morphology and flake structure of the material are uneven, which comprises large and small pieces, probably because at high concentrations, the aggregates formed are uneven, large and small, resulting in uneven material morphology. This phenomenon shows that the surfactant concentration slightly affects the morphology

of the materials, but the concentration should not be too large to prevent uneven material morphology. Therefore, the surfactant amount used herein is 0.05 g (1.25 mg/mL).

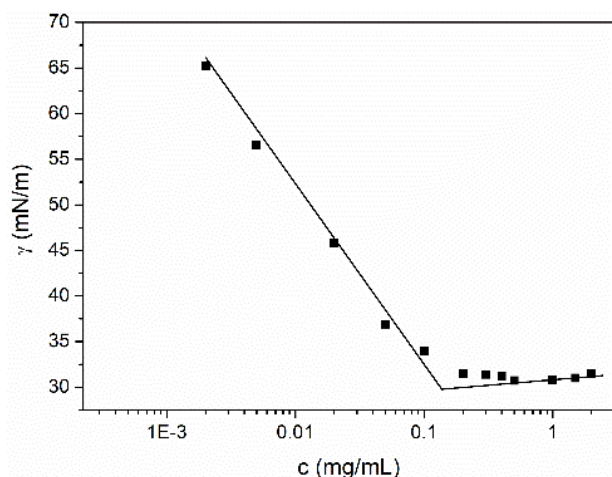


**Figure 9.** Relationship between concentration and surface tension of GC-A

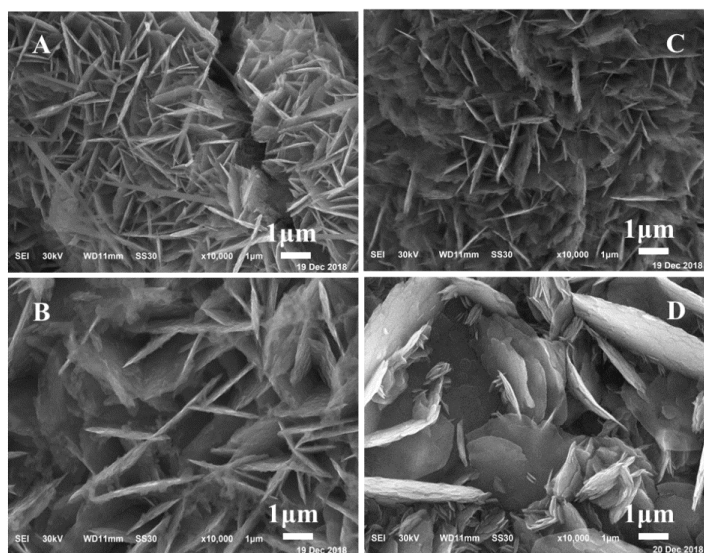


**Figure 10.** The SEM images of  $\text{NiCo}_2\text{O}_4/\text{NF}$  material were prepared adding different concentration GC-A. A: 0.5 mg/L, B: 1 mg/L, C: 2 mg/L, D: 3 mg/L

The above SEM images reveal that at low reaction temperatures ( $< 100^\circ\text{C}$ ), the material morphology comprises sheet structures. However, at high reaction temperatures ( $> 100^\circ\text{C}$ ), the material morphology comprises needle-like structures.  $\text{NiCo}_2\text{O}_4/\text{NF}$  composites formed by adding different surfactants can form sea urchin-like, needle-like, and multilayer flake structures and other structures under specific reaction conditions. The results reveal that different types of surfactants can regulate the

morphology of NiCo<sub>2</sub>O<sub>4</sub>/NF materials at different temperatures, which lays the foundation for obtaining excellent electrochemical properties.

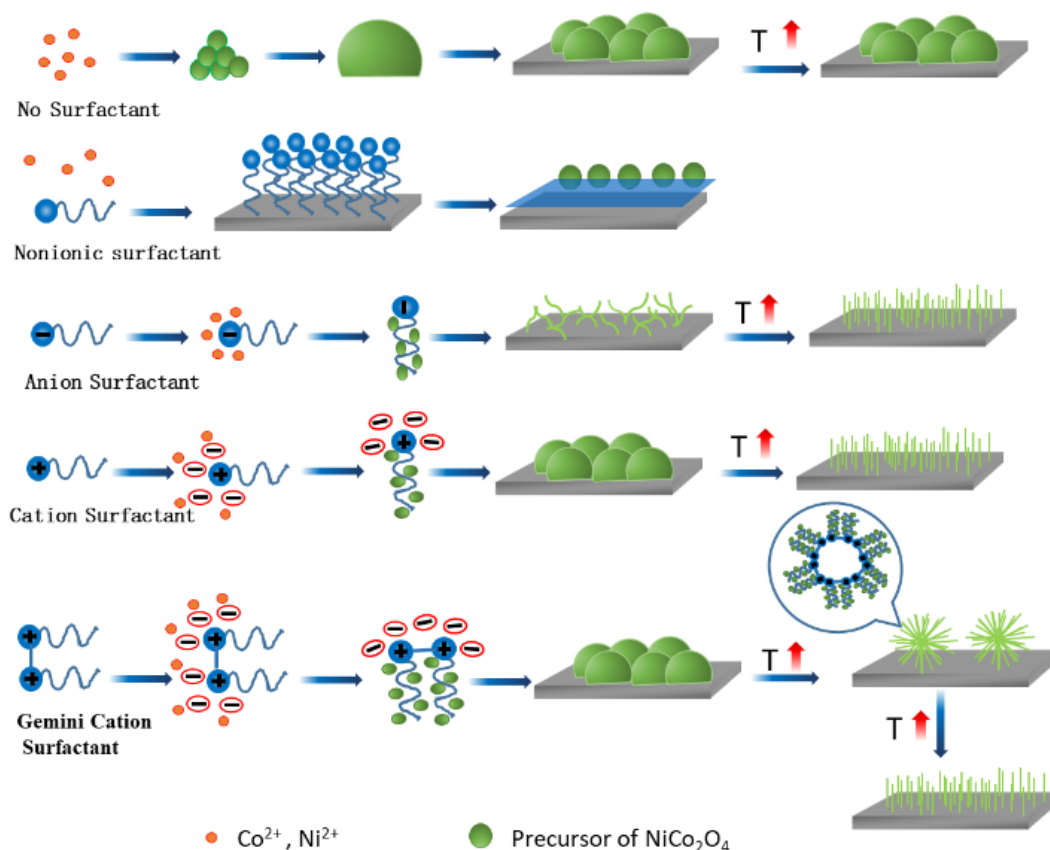


**Figure 11.** Schematic illustration for the possible mechanism of NiCo<sub>2</sub>O<sub>4</sub>/NF morphology

Several factors may exist in the formation of special structures, such as hydrogen bonds, van der Waals forces, electrostatic and dipole fields, crystal surface attraction, and inherent crystal shrinkage. It has been reported that shape-controlled crystal growth can be achieved by controlling the growth kinetics [29]. If there is no organic additive, surfactant, or any template in the reaction, the concentration of CO<sub>3</sub><sup>2+</sup>, Ni<sup>2+</sup>, and OH<sup>-</sup> plays a key role. Therefore, it may be more convincing to explain this process using directionally attached crystals. With the reaction of CO<sub>3</sub><sup>2-</sup> and OH<sup>-</sup> anions produced by urea hydrolysis with CO<sup>2+</sup> and Ni<sup>2+</sup> cations, primary nuclei form in the initial reaction stage. The newly formed nanonucleus are thermodynamically unstable due to their high surface energies. They tend to gather to minimize the interfacial energy. Therefore, the supersaturated nuclei can gather to form a sheet structure. An increase in the reaction temperature slightly affects the formation of the sheet structure (Fig. 11). However, in the presence of nonionic surfactants, NiCo<sub>2</sub>O<sub>4</sub> materials cannot form on the surface of the Ni foam. It has been reported that polyvinylpyrrolidone (PVP) is also a nonionic surfactant and a common soft template. It regulates nucleation and grain growth by coordinating the -N and C=O functional groups in the molecule and metal ions to guide the formation of products [30, 31]. The

molecular structures of APG and AEO<sub>9</sub> have neither –N and C=O functional groups nor any charge, so they cannot coordinate or adsorb with metal ions. Moreover, APG and AEO<sub>9</sub> form a thin film on the foamed nickel surface, thus impeding the adsorption of NiCo<sub>2</sub>O<sub>4</sub> on the surface of the Ni foam. The results show that NiCo<sub>2</sub>O<sub>4</sub> did not grow on the Ni foam. SNS-80 [32] due to oil-based macromolecule. Although it has been sulfonated, the sulfonation rate is low, and there are several ethoxy groups (EO) in the molecule, which reduces the charge density of the surfactant ions, thereby weakening the performance of the anions, making their properties close to nonionic properties. No –N functional group exists in the molecular structure. Although there are few C=O functional groups, it is difficult for C=O functional groups to coordinate with the metal ions due to the large molecular weight. Therefore, the film formation on the surface of the Ni foam impedes the adsorption of the metal ions (Fig. 11).

In the presence of K12, the hydrophilic terminal directly adsorbs CO<sup>2+</sup> and Ni<sup>2+</sup>. Then, CO<sup>2+</sup> and Ni<sup>2+</sup> nucleate and grow along the hydrophobic chain of K12. The distance between the anionic molecules increases due to electrostatic repulsion, and the volume between the hydrophilic and hydrophobic ends is almost parallel. At this time, the NiCo<sub>2</sub>O<sub>4</sub> of the Ni foam surface tends to form a nanowire structure. As the reaction temperature increases, the growth of the nanowires increases, so the nanowires formed are longer (Fig. 11). K12 is a typical linear anionic surfactant. However, AES contains 2–3 ethoxy groups in its molecular structure; such groups increase the hydrophilic group, and the hydrophobic chain is bent, resulting in the formation of flaky structures at low reaction temperatures. As the reaction temperature increases, the hydrophobic chain extends and tends to form nanowire structures on the surface of the Ni foam (Fig. 11).

In the presence of cationic surfactants, the hydrophilic groups of the cations first adsorb the anions (such as NO<sup>3-</sup> and OH<sup>-</sup>) in the solution, so that the hydrophilic end distance between the surfactant molecules increases and the hydrophobic ends are close to each other, resulting in the tendency to form sheet structures. As the reaction temperature increases, the kinetic energy of the cationic molecules increases, the distance between molecules decreases, the electrostatic repulsion increases, and the arrangement between molecules is parallel to each other. At this time, the NiCo<sub>2</sub>O<sub>4</sub> of the Ni foam surface tends to form nanowire structures. The Gemini cationic surfactant (GC-A) has two hydrophobic chains and two hydrophilic head groups [33]. At a reaction temperature of 140°C, the kinetic energy of the cationic molecules increases, the distance between molecules decreases, and the electrostatic repulsion increases. Furthermore, the hydrophilic head groups are close to each other, the hydrophobic chain elongates, so it is easy to form a sphere, and the material morphology becomes sea urchin-like microspheres. As the reaction temperature increases, the kinetic energy of the molecules increases, the electrostatic repulsion increases, and the hydrophobic chain is also in a parallel state, so a linear morphology is formed (Fig. 11).

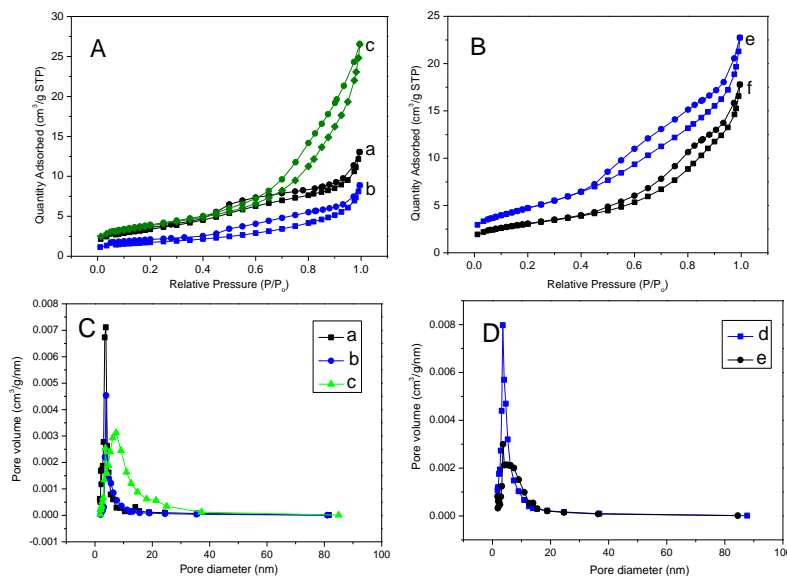


**Figure 12.**  $N_2$  adsorption isotherms and pore distribution, a: 0; b: K12; c: AES; d: GC-A; e: DMHAC10

Furthermore, the nitrogen adsorption–desorption analysis of the  $NiCo_2O_4/NF$  composites prepared by adding different surfactants was conducted at a reaction condition of  $100^\circ C$  for 6 h. The following surfactants were added: no surfactant, K12, AES, DMHAC10, and GC-A, respectively. Table 1 and Fig. 12 show that with no surfactant, the specific surface area and pore volume of the  $NiCo_2O_4/NF$  materials are small. However, with the addition of surfactants, the specific surface area and pore volume of the materials increase. Especially, the addition of the Gemini double-chain surfactant (GC-A) results in a large specific surface area and pore volume, indicating that the  $NiCo_2O_4/NF$  composites prepared by adding soft template GC-A may have better electrochemical properties.

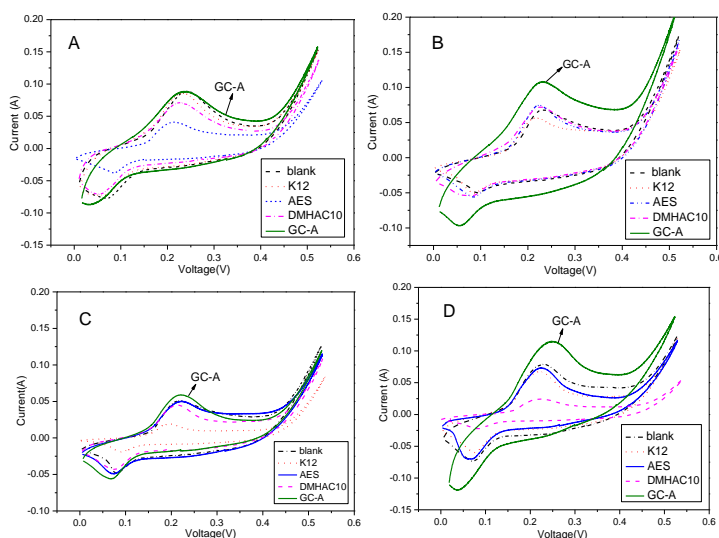
**Table 1.** Data of BET surface area and pore structure of  $NiCo_2O_4/NF$

surfactant	BET Surface Area ( $m^2/g$ )	Volume of pores ( $cm^3/g$ )	BJH Pore Diameter (nm)
a: 0	12.08	0.021	6.39
b: K12	5.92	0.014	9.80
c: AES	13.39	0.042	11.29
d: GC-A	17.29	0.036	7.07
e: DMHAC10	10.71	0.028	9.51

### 3.3 Electrochemical performance

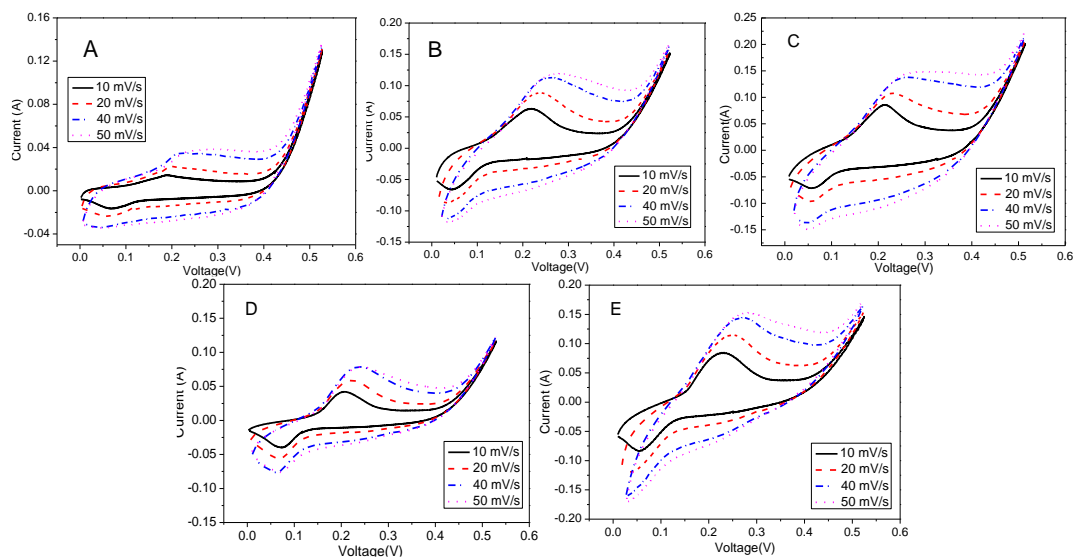
The above SEM images reveal that the addition of different surfactants can regulate the morphology of the  $NiCo_2O_4/NF$  materials at different reaction temperatures. Different surfactants have different effects, resulting in different morphologies of the materials and different electrochemical

properties. Therefore, the electrochemical properties of the composites prepared by adding different surfactants were studied.



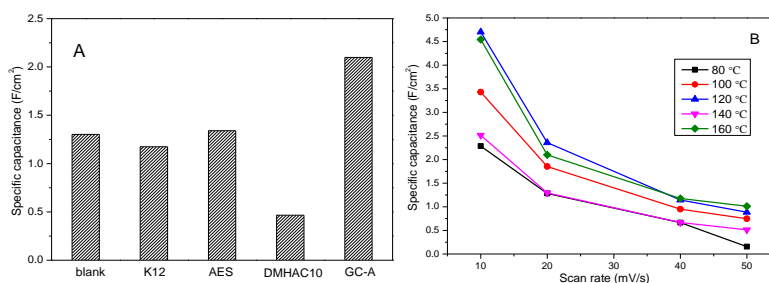
**Figure 13.** CV diagram of NiCo<sub>2</sub>O<sub>4</sub>/NF prepared by adding different surfactants. A: 100 °C; B: 120 °C; C: 140 °C; D: 160 °C.

Fig. 13 shows the CV curves of the electrode materials prepared at 100 °C, 120 °C, 140 °C, and 160 °C for 6 h in the presence of different surfactants with a scanning rate of 20 mV/s. Evidently, a pair of redox peaks exists between 0.0 and 0.10 V and 0.2 and 0.25 V, corresponding to the electrochemical redox reaction of Co<sup>3+</sup>/Co<sup>4+</sup> and Ni<sup>2+</sup>/Ni<sup>3+</sup> in the presence of OH<sup>-</sup>. This trend shows that the NiCo<sub>2</sub>O<sub>4</sub>/NF composite electrode material obeys the Faraday storage principle [34]. Comparing the CV curves of each sample (Fig. 13(A)) reveals that the CV curve area of NiCo<sub>2</sub>O<sub>4</sub>/NF prepared by adding GC-A is the largest. The results show that the specific capacitance of the NiCo<sub>2</sub>O<sub>4</sub>/NF material prepared by adding GC-A as the soft template is high, which is probably because the needle array structure prepared under the soft template has a rich pore structure and more quality electroactive substances. Also, the adsorption and desorption data in Table 1 reveal that the NiCo<sub>2</sub>O<sub>4</sub>/NF material prepared by adding GC-A has the largest specific surface area, so it can be used as an ion buffer to provide a large volume of continuous electron transport channel for electrolyte ions. The redox peak of the NiCo<sub>2</sub>O<sub>4</sub>/NF composite electrode material prepared by adding GC-A as the soft template agent and the maximum area of the CV curve at 120 °C and 160 °C are also evident. The main reason was that the nanostructure of the NiCo<sub>2</sub>O<sub>4</sub>/NF material prepared at this temperature was more compact, and it had more quality electroactive materials.



**Figure 14.** CV diagram of NiCo<sub>2</sub>O<sub>4</sub>/NF prepared by adding GC-A. A: 80 °C; B: 100 °C; C: 120 °C; D: 140 °C; E: 160 °C.

Fig. 14(A)–(E) show the CV curves of NiCo<sub>2</sub>O<sub>4</sub>/NF prepared with GC-A at 80 °C, 100 °C, 120 °C, 140 °C, and 160 °C at different scanning rates. Evidently, a pair of significant electrochemical redox peaks occur in the range of scanning rate from 10.0–50.0 mV/s. Also, the CV curves under different scanning rates were compared. As the scanning rate increases, the electrochemical anode and cathode peaks of all samples shift to red and blue, respectively. As shown in Fig. 14(E), when the scanning speed increases from 10.0 to 50.0 mV/s, the anode peak of NiCo<sub>2</sub>O<sub>4</sub>/NF shifts from 0.06 to 0.04 V, and the change value is 20.0 mV. The cathode peak shifts from 0.24 to 0.26 V, and the change value is 20.0 mV. Although the scanning rate increased by five times, the changes in the anode and cathode peaks were minimal. These results show that the NiCo<sub>2</sub>O<sub>4</sub>/NF materials prepared under these conditions have good electrochemical stability characteristics.



**Figure 15.** A: The special capacity of the NiCo<sub>2</sub>O<sub>4</sub>/NF; B: Relation between scan rate and specific capacitance

Fig. 15(A) shows the specific capacitance of the NiCo<sub>2</sub>O<sub>4</sub>/NF materials prepared using different soft templates at 160 °C at a scanning speed of 20 mV/s. Evidently, the maximum-specific capacitance

of NiCo<sub>2</sub>O<sub>4</sub>/NF prepared by adding GC-A is 2.307 F/cm<sup>2</sup>, followed by 1.423 F/cm<sup>2</sup> for the electrode material prepared with no soft template. This disparity occurs because the fibrous structure has a more electroactive area than the simple sheet structure. Also, the specific capacitance of NiCo<sub>2</sub>O<sub>4</sub>/NF prepared by adding GC-A as the soft template at different reaction temperatures decreases as the scanning speed increases (Fig. 15(B)). At a scanning speed of 10 mV/s, the maximum-specific capacitance of NiCo<sub>2</sub>O<sub>4</sub>/NF prepared at 120°C is 4.743 F/cm<sup>2</sup>. As the scanning speed increases, the specific capacitance of the electrode material prepared at 120°C slightly exceeds that at 160°C, and the specific capacitance is similar at 40 mV/s. At a scanning speed of 50 mV/s, the specific capacitance at 160°C exceeds that at 120°C. The results show that the specific capacitance retention of NiCo<sub>2</sub>O<sub>4</sub>/NF prepared by adding GC-A at high temperature was better, which lays the foundation for improving the charging speed.

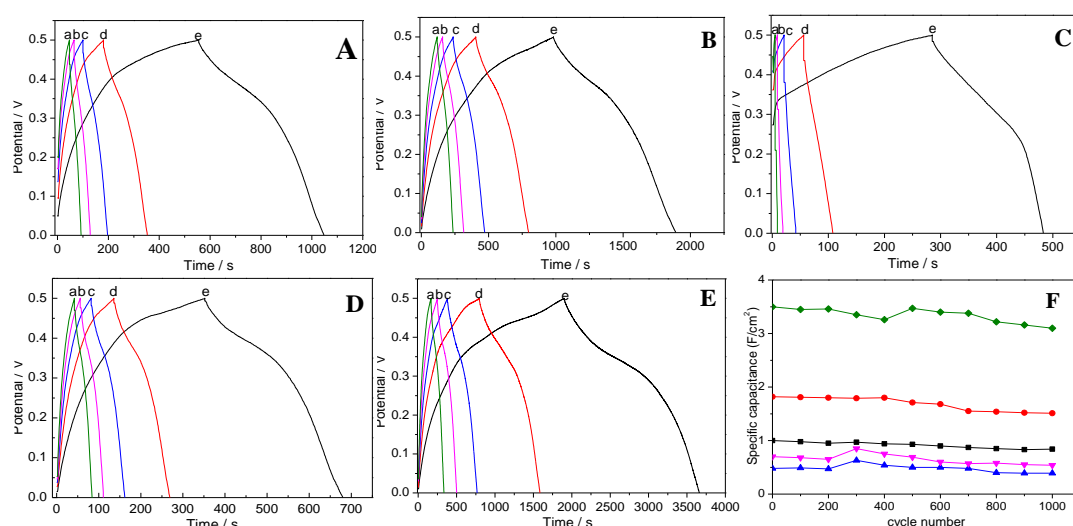


**Figure 16.** The GCD curves of the NiCo<sub>2</sub>O<sub>4</sub>/NF prepared in presence of (A)No surfactant, (B)K12, (C)AES, (D) DMHAC10 and (E) GC-A at various current densities; (F) Relationship between specific capacity and charge discharge times. (a) 5.0 mA/cm<sup>2</sup>; (b) 4.0 mA/cm<sup>2</sup>; (c) 3.0 mA/cm<sup>2</sup>; (d) 2.0 mA/cm<sup>2</sup>; (e) 1.0 mA/cm<sup>2</sup>. ■ no surfactant; ● K12; ▲ AES; ▼ DEQ; ◆ GC-A.

The electrochemical storage performance characteristics of the NiCo<sub>2</sub>O<sub>4</sub>/NF materials were further characterized by the charge–discharge curves. Fig. 16(A)–(E) shows the constant current charge–discharge curves of NiCo<sub>2</sub>O<sub>4</sub>/NF prepared at a reaction condition of 120°C for 6 h with different soft templates and at varying current densities. Evidently, the specific electric capacities of the NiCo<sub>2</sub>O<sub>4</sub>/NF materials prepared with no surfactant, K12, AES, DMHAC10, and GC-A are 1.0, 1.82, 0.48, 0.7, and 3.5 F/cm<sup>2</sup> respectively. The specific capacitance of NiCo<sub>2</sub>O<sub>4</sub>/NF prepared by adding GC-A is the highest, which is consistent with the CV results. At current densities of 1.0, 2.0, 3.0, 4.0, and 5.0 mA/cm<sup>2</sup>, the specific capacities of NiCo<sub>2</sub>O<sub>4</sub>/NF prepared by GC-A are 3.5, 3.2, 2.4, 2.1, and 1.8 F/cm<sup>2</sup>, respectively. As the current density increases from 1.0 to 5.0 mA/cm<sup>2</sup>, the specific capacitance of NiCo<sub>2</sub>O<sub>4</sub>/NF decreases by 49.1%. The results show that when the current density increases five times, 66.0%, 50.0%, 61.4%, and 50.9% of the specific capacitance of the NiCo<sub>2</sub>O<sub>4</sub>/NF materials prepared with K12, AES,

**Table 2.** Comparison of electrochemical properties of different NiCo<sub>2</sub>O<sub>4</sub> materials

Appearance	Preparation method	Specific capacitance	Cycle stability	Refs
NiCo <sub>2</sub> O <sub>4</sub> /NF mixed morphology of cactus	Hydrothermal method	3.5 F/cm <sup>2</sup>	88.6% (1000 cycles)	This work
NiCo <sub>2</sub> O <sub>4</sub> nanorods	Grinding	0.565 F/cm <sup>2</sup>	77.6% (1000 cycles)	35
3D multistage flower NiCo <sub>2</sub> O <sub>4</sub> microspheres	Microwave assisted reflux method	3.018 F/cm <sup>2</sup>	93.2% (1000 cycles)	36
Coralline NiCo <sub>2</sub> O <sub>4</sub>	Sol-gel method	1.215 F/cm <sup>2</sup>	96.3% (600 cycles)	37
NiCo <sub>2</sub> O <sub>4</sub> stacked nanostructure	D-glucose-assisted solvothermal process	0.452 F/cm <sup>2</sup>	92 % (2500 cycles)	38
NiCo <sub>2</sub> O <sub>4</sub> double-shell hollow spheres	Programmed coating of carbon spheres	2.27 F/cm <sup>2</sup>	85.8% (2000 cycles)	39
NiCo <sub>2</sub> O <sub>4</sub> nanoparticles	Hydrothermal and softtemplating method	1.92 F/cm <sup>2</sup>	65% (100 cycles)	40

DMHAC10, and GC-A are retained, respectively, which shows that the electrode material with multistage structures has a better charge–discharge ratio. Fig.16 (F) shows the relationship between the specific capacitance and the charge–discharge times of the NiCo<sub>2</sub>O<sub>4</sub>/NF materials prepared at a reaction condition of 120°C for 6 h at 1.0-mA/cm<sup>2</sup> current density. Evidently, after 1000 charge–discharge cycles of the NiCo<sub>2</sub>O<sub>4</sub>/NF materials prepared without surfactant, K12, AES, DMHAC10, and GC-A, the specific capacitance values are 0.84, 1.51, 0.39, 0.54, and 3.1 F/cm<sup>2</sup>, respectively, which are 84.0%, 83.0%, 81.3%, 77.4%, and 88.6% of the initial specific capacitance. These results show that the NiCo<sub>2</sub>O<sub>4</sub>/NF material prepared by adding GC-A as the soft template exhibits good electrochemical cycle stability. By comparing the specific capacitance and cycle stability of other NiCo<sub>2</sub>O<sub>4</sub> materials, it was found that the NiCo<sub>2</sub>O<sub>4</sub>/NF mixed morphology of cactus exhibited largest specific capacitance and better cycle stability as shown in Table 2.

#### 4. CONCLUSIONS

Herein, several self-supporting NiCo<sub>2</sub>O<sub>4</sub>/NF materials with different dimensions, different morphologies, and excellent electrochemical properties were successfully prepared by adjusting the type of surfactant and reaction temperature. The relationships between the reaction temperature, surfactant structure, morphology, and electrochemical properties of the NiCo<sub>2</sub>O<sub>4</sub>/NF materials were systematically studied, and their morphological growth mechanisms were discussed. The results show that: (1) CO<sup>2+</sup> and Ni<sup>2+</sup> adsorbed at the hydrophilic end of the linear anionic surfactant can nucleate and grow along the hydrophobic chain. The molecular structure of the surfactant was almost parallel due to electrostatic repulsion. NiCo<sub>2</sub>O<sub>4</sub>/NF materials tend to form nanowire structures on NF. As the reaction temperature increased, the growth of the nanowires was better. (2) The hydrophilic groups in the cationic surfactants

adsorb the anions in the solution, increasing the hydrophilic end distance between the surfactant molecules. Thus, the hydrophobic ends were close, resulting in the tendency to form sheet structures. As the temperature increased, the molecular kinetic energy increased, the distance between molecules decreased, the electrostatic repulsion increased, and the arrangement between molecules was close to parallel. NiCo<sub>2</sub>O<sub>4</sub>/NF tends to form nanowire structures on the Ni foam. (3) Nonionic surfactants hinder the growth of NiCo<sub>2</sub>O<sub>4</sub> on the Ni foam. Counter ions only affect the size of the material structure, but have no effect on the material morphology, and the concentration of surfactant has little effect on the material morphology. (4) The electrochemical performance results show that the cactus spherical three-dimensional (3D) NiCo<sub>2</sub>O<sub>4</sub>/NF materials prepared by adding GC-A can be used as an ion buffer library to provide a large-volume 3D continuous electron transport channel for electrolyte ions, giving the materials higher conductivity and better structural and mechanical stabilities. Under the reaction condition of 120°C for 6 h, the materials have excellent electrochemical properties, such as better specific capacity (4.74 F/cm<sup>2</sup>), excellent charge–discharge ratio, and storage stability. (5) This study provides a new strategy for accurately designing NiCo<sub>2</sub>O<sub>4</sub>/NF with different morphologies.

#### ACKNOWLEDGMENT

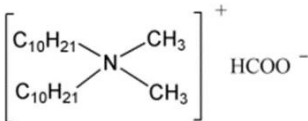
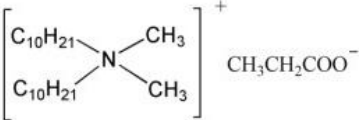
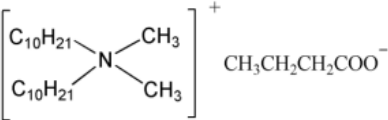
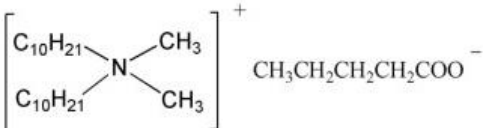
This work was supported by the National Natural Science Foundation of China (No. 22002105), the Science and Technology Innovation Project of Colleges and Universities in Shanxi Province (No. 2020L0355)

#### CONFLICTS OF INTEREST

The authors declare that they have no competing interests.

#### SUPPORTING INFORMATION

**Tab S1.** Name and molecular structure of surfactants

Serial number	Surfactant name(abbreviation)	Structural formula
1	N-Decyl-N,N-dimethyldecyl-1-aminium formate (DDAF)	
2	N-Decyl-N,N-dimethyldecyl-1-aminium propionate (DDAP)	
3	N-Decyl-N,N-dimethyldecyl-1-aminium butyrate (DDAB)	
4	N-Decyl-N,N-dimethyldecyl-1-aminium valerate (DDAV)	

5	N-Decyl-N-(2-hydroxyethyl)-N-methyldecyl-1-aminium chloride (DMHAC10)	
6	N-Decyl-N,N-dimethyldecyl-1-aminium chloride (DDAC)	
7	N, N-dimethyl dodecyl/tetradecyl tertiary amine Gemini (GC-A)	
8	Alkyl glycoside 12-14 (APG12/14)	
9	Fatty alcohol polyoxyethylene ether (AEO9)	$C_{12}H_{25}O(C_2H_4O)_n$ $n=9$
10	Fatty alcohol polyoxyethylene ether sulfate (AES)	$RO(CH_2CH_2O)_n-SO_3Na$ ( $n=2$ or $3$ , $R=C_{12}H_{25}/C_{14}H_{29}$ )
11	Sodium dodecyl sulfate (K12)	$CH_3(CH_2)_{11}OSO_3Na$
12	Modified oil ethoxylate sodium sulfonate (SNS-80)	The modified oil is added with a certain amount of ethylene oxide and then sulfonated, which belongs to macromolecular products.

## References

1. N. Garg, M. Basu, K. Upadhvay, S. M. Shivaprasad and A. K. Ganguli, *RSC Adv.*, 3 (2013) 24328.
2. G. Huang, L. Zhang, *Nanoscale*, 6 (2014) 5509.
3. K. Sun, Y. Q. Zhao, J. Yin, J. Jin, H. W. Liu and P. X. Xi, *Acta Phys. -Chim. Sin.*, 6 (2022) 2107005.
4. Y. L. Tong, M. Z. Dai, L. Xing, H. Q. Liu, W. T. Sun and X. Wu, *Acta Phys. -Chim. Sin.*, 36 (2020) 1903046.
5. S. Y. Yang, J. Yu, T. T. Jiang, L. X. Zhu and X. L. Xu, *J. Alloys. Compd.*, 764 (2018) 767.
6. X. Y. Hou, S. Xue and M. T. Liu, *Chem. Eng. J.*, 350 (2018) 29.
7. X. H. Qi, W. J. Zheng, G. He, T. Tian and L. Wang, *Chem. Eng. J.*, 309 (2017) 426.
8. H. Hentze, S. R. Raghavan, C. A. Mckelvey and E. W. Kaler, *Langmuir*, 19 (2003) 1069.
9. Y. Li, L. Zou, J. Li, K. Guo and Y. Hui, *Electrochim. Acta.*, 129 (2014) 14.
10. P. Valeri, L. Youngmin, S. H. Sun and Y. Ren, *J. Phys. Chem. C.*, 116 (2012) 26668.
11. C. C. Zhou and Y. L. WANG, *Curr. Opin. Colloid Interface Sci.*, 45 (2020) 28.
12. J. Y. Xiao and L. M. Qi, *Acta Phys. -Chim. Sin.*, 36 (2020) 1910001.
13. J. J. Zhang, Q. W. Mei, Y. P. Ding, K. Guo, X. X. Yang and J. T. Zhao, *ACS Appl. Mater. Interfaces*, 9 (2017) 29771.
14. L. L. Liu and Y. WANG, *J. Changchun Nor. Univ. (Nat. Sci.)*, 3 (2014) 62.
15. S. X. Xing, L. H. Tan, M. X. Yang, M. Pan, Y. B. Lv, Q. H. Tang, Y. H. Yang and H. Y. Chen, *J. Mater. Chem.*, 19 (2009) 3286.
16. C. C. Zhou, F. Y. Wang, H. Chen, M. Li, F. L. Qiao, Z. Liu, Y. B. Hou, C. X. Wu, Y. X. Fan, L. B. Liu, S. Wang and Y. L. Wang, *ACS Appl. Mater. Interfaces*, 8 (2016) 4242.
17. J. Mi and W. C. Li, *Chin. J. Power Sources*, 7 (2014) 1394.
18. L. H. Bao, J. F. Zhang and X. D. Li, *Nano Lett.*, 11 (2011) 1215.
19. L. Zhang, C. M. B. Hilt, E. J. Luber, B. C. Olsen, H. Wang, M. Danaie, X. Cui, X. H. Tan, V. W.

- Lui and W. P. Kalisvaart, *J. Phys. Chem. C.*, 115 (2011) 24381.
20. J. H. Mou, G. Z. Li, H. C. Xiao, Y. Liu, L. Huang and B. Q. Li, *Chin. Sci. Bull.*, 46 (2001) 1.
  21. H. L. Li, P. Idabelle, G. Theophile and D. Audrey, *Colloids Surf., A.*, 540 (2018) 167
  22. C. G. Wang, E. Zhou, W. D. He, X. L. Deng, J. Z. Huang, M. Ding, X. Q. Wei, X. J. Liu and X. J. Xu, *Nanomaterials*, 7 (2017) 41.
  23. S. S. Yao, L. F. Zhi, J. Guo, S. J. Yan and M. G. Zhang, *Int. J. Electrochem. Sci.*, 13 (2018) 542.
  24. S. S. Yao, L. F. Zhi, J. Guo, S. J. Yan and M. G. Zhang, *Micro. Nano. Lett.*, 13 (2018) 821.
  25. C. Jin, F. Lu, X. C. Cao, Z. R. Yang and R. Z. Yang, *J. Mater. Chem. A.*, 1 (2013) 12170.
  26. Z. Peng and A. M. Alenizi, *Adv. Energy Mater.*, 5 (2015) 1042031.
  27. W. Y. Tang, T. Geng, Y. J. Jiang, H. B. Ju and Z. L. Dong, *Fine Chem.*, 32 (2015) 1106.
  28. J. F. Sun, Q. X. Li and Y. L. Li, *Fine Chem.*, 25 (2008) 565.
  29. E. P. Barrett, L. G. Joyner and P. P. Halenda, *J. Am. Chem. Soc.*, 73 (1951) 373.
  30. Y. R. Zhu, J. F. Wang, Z. B. Wu, M. J. Jing, H. S. Hou, X. N. Jia and X. B. Ji, *J. Power Sources*, 287 (2015) 307.
  31. L. L. Li, Y. L. Cheah, Y. Ko, P. F. Teh, G. Wee, C. L. Wong, S. J. Peng and M. Srinivasan, *J. Mater. Chem. A.*, 1 (2013) 10935.
  32. H. B. Liang, J. J. Zhou, Y. Q. Sun, Y. Zhang, J. Y. Sun and L. R. Ding, *Deter. Cosmetics*, 42 (2019) 38.
  33. Y. X. Wang, M. L. Deng, Y. Q. Tang, Y. C. Han, X. Huang, Y. B. Hou and Y. L. Wang, *Acta. Phys. - Chim. Sin.*, 36 (2020) 1909046.
  34. S. M. Sun, S. Wang, S. D. Li, Y. N. Li, Y. H. Zhang, J. L. Chen, Z. H. Zhang, S. M. Fang and P. Y. Wang, *J. Mater. Chem. A.*, 4 (2016) 1.
  35. Y. R. Zhu, X. L. Pu, W. X. Song, Z. B. Wu, Z. Zhou, X. He, F. Lu, M. J. Jing, B. Tang and X. B. Ji, *J. Alloy. Compd.*, 617 (2014) 988.
  36. Y. Lei, J. Li, Y. Wang and L. Gu, *ACS Appl. Mater. Interfaces*, 6 (2014) 1773.
  37. Q. W. Ye, Y. C. Xiang and T. J. Ping, *Electrochim. Acta.*, 56 (2011) 7517.
  38. N. Padmanathan and S. Selladurai. *Ionics*, 19 (2013) 1535.
  39. X. Li, L. Jiang and C. Zhou, *NPG Asia Mater.*, 7 (2015) 165.
  40. R. Ding, L. Qi, M. J. Jia and H. Y. Wang, *J. Appl. Electrochem.*, 43 (2013) 903.